Ballistic Acceleration of a Supercurrent in a Superconductor

Gabriel F. Saracila and Milind N. Kunchur*

Department of Physics and Astronomy, University of South Carolina, Columbia, South Carolina 29208, USA

(Received 26 October 2008; published 17 February 2009)

One of the most primitive but elusive current-voltage (I-V) responses of a superconductor is when its supercurrent grows steadily after a voltage is first applied. The present work employed a measurement system that could simultaneously track and correlate $I(t)$ and $V(t)$ with subnanosecond timing accuracy, resulting in the first clear time-domain measurement of this transient phase where the quantum system displays a Newtonian like response. The technique opens doors for the controlled investigation of other time-dependent transport phenomena in condensed-matter systems.

DOI: 10.1103/PhysRevLett.102.077001 PACS numbers: 74.25.Op, 72.15.Lh, 74.25.Fy, 74.25.Qt

A particle under the action of a single applied force accelerates ballistically in accordance with Newton's second law. In the presence of a frictional force, an applied force will ultimately maintain a constant velocity rather than produce acceleration. Analogously, an externally applied voltage V maintains a constant current I in the case of a resistive conductor, whereas it can ballistically accelerate the superfluid in a superconductor, leading to a supercurrent that grows with time. This acceleration phase of the supercurrent lasts for a very brief period—until flux motion, phase slip centers, or other dissipative phenomena set in—making it extremely difficult to observe in the time domain in a correlated current-voltage measurement. In the present work, an electrical measurement system was developed that could resolve and correlate the time evolutions of $I(t)$ and $V(t)$ on a subnanosecond time scale. For the sample pattern, extremely long meander geometries (with length-to-width aspect ratios in the thousands) were employed to prolong the acceleration time while maintaining V at a manageable level. The combination of these two measures facilitated the successful observation of the acceleration phase.

The acceleration of the supercurrent density j_s is given by (from the London equations [1,2])

$$\frac{dj}{dt} \simeq \frac{dj_s}{dt} = \frac{Ee^2 n_s}{m^*} = \frac{E}{\mu_0 \lambda_L^2}, \tag{1}$$

where E is the local internal electric field, e is the electronic charge, m^* is the effective mass, and n_s is the superfluid density (related to the number of electrons per volume participating in the condensate); the far right-hand side of the equation relates n_s to the London magnetic-field penetration depth λ_L; we can take $j = j_s + j_n \simeq j_s$ because the normal current density j_n is a negligible component of the total current density j. This supercurrent acceleration phase lasts for the duration $\Delta t \approx j_c \mu_0 \lambda_L^2 / E$, where j_c is the critical current density that marks the onset of resistance. The inductance-like proportionality between dj/dt and E in Eq. (1), arising from the inertia of the superfluid, is referred to as the kinetic inductance L_k. In terms of the geometrical length l and cross sectional area A, it is given by

$$L_k = \frac{\mu_0 \lambda^2 l}{A}, \tag{2}$$

where λ is a more general penetration depth, which includes effects such as impurity scattering ($\lambda \geq \lambda_L$). Kinetic inductive effects are small except close to the transition temperature T_c, where their signatures have been seen in the high-frequency ac response or as nonequilibrium inductive voltage spikes during abrupt current steps [3–11]. In the present work, time scales were chosen to be short enough to have a sufficient magnitude of V while long enough (compared to characteristic time scales such the gap-relaxation and electron-phonon scattering times) to avoid nonequilibrium effects. Variations in fields occurred at length scales that were long compared with both λ and the coherence length ξ, so as to avoid nonlocal effects. Thus, the conditions were optimum for observing the simplest limiting behavior of an accelerating condensate as predicted by the London equations, i.e., Eq. (1).

The samples used in this work were niobium films deposited on silicon substrates with DC magnetron sputtering. The films were patterned into long narrow meanders by electron-beam lithography using the lift-off technique. Sample A had a thickness of $t = 70 \pm 8$ nm, a width of $w = 12.1 \pm 0.6$ μm, and a length (between voltage probes) of $l = 4.80 \pm 0.01$ cm. Sample B had the dimensions $t = 85 \pm 8$ nm, $w = 8.9 \pm 0.6$ μm, and $l = 4.53 \pm 0.01$ cm. Their respective superconducting transition temperatures were $T_c = 6.74$ K and $T_c = 7.23$ K.

The measurements were carried out in a pulsed-tube closed-cycle refrigerator in zero applied magnetic field. The electrical measurements were conducted with a pulsed signal source and detection electronics, in combination with a digital storage oscilloscope. Parts of the signal-source and preamplifier circuitry in this setup were developed and built inhouse. An active (buffered) ground arrangement was developed for improving the shielding between the fast changing high-voltage signal in the cur-

rent leads from the low-voltage sample-signal sensing leads. The entire signal chain up until the digital oscilloscope is analog. Using pulsed signals instead of continuous ac or dc excitations permits a wider range of currents without Joule heating of the sample and a flexible control over the waveform shape. The system performs simultaneous independent differential four-probe measurements of $I(t)$ and $V(t)$ with a relative timing accuracy of $\sim$100 ps. The stray mutual inductive coupling between current and voltage leads has a (temperature independent) value of $\lesssim$1 nH (the self inductances of the leads themselves are not sensed because of the four-probe configuration). The absolute accuracy of the inductance values measured in this system is about $\pm 5\%$. The voltage-measurement sensitivity is about 1 μV. The time interval between digitized samples is 10^{-10} second (the single-shot digitizing sampling rate is 10 gigasamples/s). The speed and accuracy with which both $I(t)$ and $V(t)$ were tracked and correlated in a superconductor in the present experiment are, to our knowledge, unprecedented.

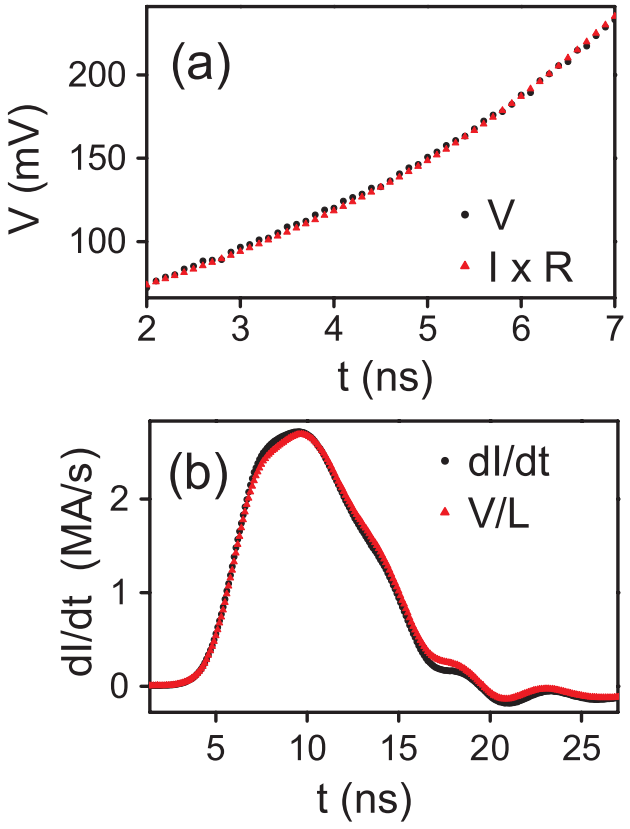

FIG. 1 (color online). Measurement-apparatus temporal accuracy checks. (a) $V(t)$ and $I(t)$ (multiplied by a constant $R = 62\ \Omega$) for a test resistor in place of a superconducting sample. (b) $dI(t)/dt$ and $V(t)$ (divided by a constant $L = 15$ nH) for a test inductor in place of a superconducting sample. The voltages across the purely resistive and inductive loads are seen to track their respective current and current-derivative functions with subnanosecond accuracy.

Some tests and verifications of the measurement system are shown in Fig. 1. Panel (a) shows the voltage and current (scaled by a constant) for a purely resistive test sample and panel (b) shows the current derivative and voltage (scaled by a constant) for a purely inductive test sample. The time scales used in the actual experiment were longer than these test conditions of Fig. 1 so that the temporal tracking between the current and voltage sensing circuits was essentially perfect. Some additional information on the apparatus can be found in our previous review articles [12,13].

Figures 2(a) and 2(b) show $V(t)$ (solid lines) across two niobium-meander samples in the superconducting state at one temperature. Panels (c) and (d) show the corresponding $I(t)$ functions, which are seen to accelerate steadily during the plateaus in $V(t)$. The dashed lines in panels (a) and (b) show dI/dt scaled by a constant ($L = 16.7$ and 16.9 nH for samples A and B, respectively) and are seen to track $V(t)$ in instantaneous detail. Thus, the response is purely inductive, with an inductance that is independent of I and dI/dt.

The ratio between the $dI(t)/dt$ and $V(t)$ curves in the top panels of Fig. 2 gives the time and current dependent inductance: $L(t) = V(t)/[dI(t)/dt]$. Figures 3(a) and 3(b) plot this $L(t)$ versus time for various values of T, for each of the samples. The plateau value of L is seen to increase steadily with temperature as is expected because of the declining superfluid density and consequent rising λ_L. Another interesting trend is that the curves at highest temperatures show $L(t)$ functions that rise with time (i.e., current). This happens because the current suppresses the superfluid density through its pair-breaking action, a regime not seen before in any other kind of measurement.

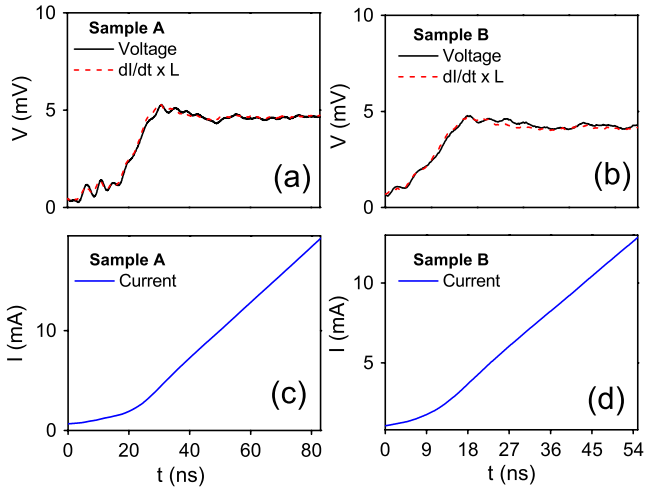

FIG. 2 (color online). Time dependencies of voltage and current in niobium meanders at $T = 3.84$ K. Panels (a) and (b) represent $V(t)$ and dI/dt (scaled by a constant L) for samples A and B, respectively. Panels (c) and (d) show the corresponding $I(t)$ functions, which rise steadily during the voltage plateaus of the panels above; the time axes for panels (a) and (c) and for panels (b) and (d) are the same.

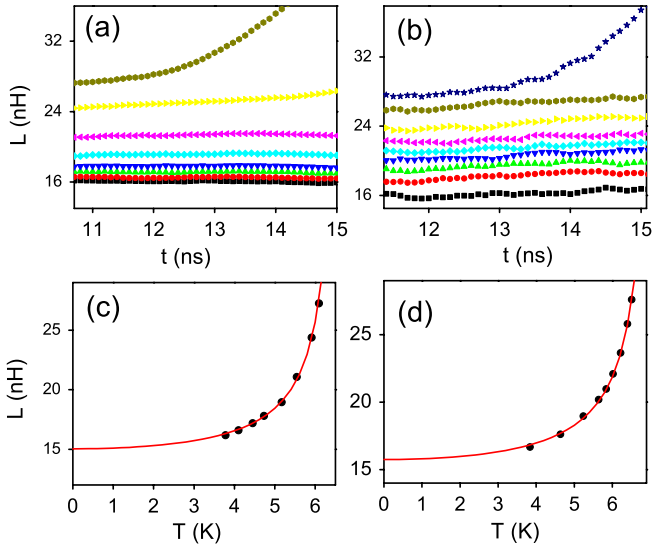

FIG. 3 (color online). (a) Measured total inductance, $L(t) = V(t).dt/dI(t)$, versus time for sample A. The curves correspond to the temperatures (from top to bottom): $T = 6.10$, 5.91, 5.54, 5.17, 4.73, 4.10, and 3.78 K. (Each plot symbol on these curves corresponds to separately measured digital voltage sample. The period between samples is 100 ps.) (b) A similar $L(t)$ plot for sample B. For this panel, the temperatures (from top to bottom) are: $T = 6.51$, 6.4, 6.22, 6.02, 5.84, 5.24, 4.64, and 3.84 K. Panels (c) and (d) show the temperature dependencies of the above measured L values (taken on the plateaus around $t \sim 11$ ns) for samples A and B, respectively. The symbols show the experimental data and the solid line represents the least-squares fit to the two-parameter function $L(T) = L_g + L_k(0)/[1 - (T/T_c)^2]$ as discussed in the text.

Note that continuous ac probes of n_s cannot endure high enough excitation levels to explore this regime because of Joule heating; and tunneling measurements reveal the spectral gap Ω_g rather than n_s. A systematic study of the suppression of n_s by j will be the subject of a future investigation, since the optimum sample geometry for studying this effect is almost opposite to the sample geometry required for the present experiment.

Figures 3(c) and 3(d) plot L (as measured above) versus T for each sample. This total inductance $L = L_k + L_g$ has components corresponding to the kinetic inductance L_k as well as a geometrical inductance L_g (from magnetic flux change). The temperature dependence arises chiefly from L_k; the changes in L_g with temperature—arising from changes in the current-density profile across the cross section—are relatively small (~4%). From Eq. (2) and the empirical temperature dependence of the penetration depth [8–10], we have

$$L_k(T) \approx \frac{L_k(0)}{[1 - (T/T_c)^2]}, \tag{3}$$

where $L_k(0) = \mu_0 \lambda^2(0) l/A$. The solid line curves in Fig. 3(c) and 3(d) correspond to a least-squares fit to the function $L(T) = L_g + L_k(0)/[1 - (T/T_c)^2]$. The values of $L_k(0)$ and L_g obtained from this fitting (T_c is not a fitting parameter) are listed in columns 2 and 4 of Table I. The coefficients of determination of the fits are $R^2 = 0.9989$ and $R^2 = 0.9994$ for samples A and B, respectively. The standard errors of the fit combined with the error in the inductance measurement gives the error bars for $L_k(0)$ that are indicated in the table.

The third and fifth columns of Table I show, for comparison, theoretical estimates of $L_k(0)$ and L_g. For finding $L_k(0)$, we note that the effective penetration depth (λ) becomes lengthened with respect to its clean-limit value (λ_L) in the presence of scattering by static disorder. This effect of impurity scattering can be incorporated through the residual resistivity ρ_0 and expressed in terms of the order parameter Δ as [14]

$$\lambda(0) = \sqrt{\frac{\hbar \rho_0}{\pi \mu_0 \Delta(0)}}. \tag{4}$$

Taking the measured values of $\rho_0 = 0.347$ $\mu\Omega$ m and 0.369 $\mu\Omega$ m, and obtaining $\Delta(0) \approx 2k_B T_c$ from our measured values of T_c, we get $\lambda = 223$ and 222 nm, and $L_k = 3.5$ and 3.7 nH for samples A and B, respectively. There is an uncertainty in the values ρ_0 because of the uncertainty in sample dimensions and an uncertainty in $\Delta(0)$ because of an uncertainty in the absolute value of T_c (this is roughly estimated to be around 200 mK). This gives rise to the error bars in the theoretical L_k values that are stated in the table. The calculated values of L_k are somewhat larger than the measured ones, but of comparable magnitude.

The theoretical geometrical inductances for the meanders, tabulated in the last column of Table I, were computed numerically by integrating the magnetic flux that links to the path between the voltage probes. The error bars in the theoretical L_g arise from the uncertainties in the sample dimensions and the approximations inherent in the calculation. It can be seen that the theoretically estimated L_g values are also in agreement with their measured counterparts.

In summary, this work has explored the initial acceleration phase during which a supercurrent builds up in response to an applied voltage. The voltage and current curves of Fig. 2 represent the first clear and direct time-domain demonstration of this primitive regime, where the quantum system shows a Newtonian like response. It is also the first time to observe the nonlinear regime where

TABLE I. Experimentally observed values and theoretically estimated values of the kinetic and geometrical inductances.

	$L_k(0)$ in (nH)		L_g in (nH)	
Sample	Expt.	Theor.	Expt.	Theor.
A	2.8 ± 0.2	3.5 ± 0.7	12.2 ± 1	15.4 ± 3
B	2.8 ± 0.2	3.7 ± 0.7	12.9 ± 1	12.0 ± 3

the current suppresses the superfluid density, thereby increasing the kinetic inductance. The instrumentation developed for this experiment is unique and represents the first measurement of its kind where both $V(t)$ and $I(t)$ are tracked in a superconductor with subnanosecond timing accuracy. This technique can reveal more detailed information than just an impulse-response measurement, and it can be used to explore time-dependent and nonequilibrium phenomena in condensed-matter systems in a controlled way (some examples of such regimes in superconductors would be those related to phase slippage, glassy dynamics, and the nascent stage of a vortex right after its nucleation). The present work and its method should be distinguished from past experiments in which an abrupt supercritical current pulse was applied [5,11] and only the subsequent $V(t)$ response was measured without monitoring $I(t)$. In those experiments, the superconductor recoils in a highly nonequilibrium manner to the supercritical stimulus. In the present study, the superconducting system is always maintained close to equilibrium by keeping the experimental time scales well in excess of the gap-relaxation and electron-phonon scattering times, while keeping the time scales short enough to observe the inertia of the superfluid.

The authors acknowledge useful discussions with J. M. Knight, B. I. Ivlev, R. A. Webb, R. J. Creswick, T. R. Lemberger, G. Simin, T. M. Crawford, and F. T. Avignone III. This research was supported by the U. S. Department of Energy through Grant No. DE-FG02-99ER45763.

*Corresponding author: kunchur@sc.edu
http://www.physics.sc.edu/kunchur

[1] F. London and H. London, Proc. R. Soc. A **149**, 71 (1935).
[2] *Introduction to Superconductivity*, edited by M. Tinkham (McGraw Hill, New York, 1996), 2nd ed.
[3] I. F. Oppenheim, S. Frota-Pessona, and M. Octavio, Phys. Rev. B **25**, 4495 (1982).
[4] A. Geier and G. Schon, J. Low Temp. Phys. **46**, 151 (1982).
[5] D. J. Frank, M. Tinkham, A. Davidson, and S. M. Faris, Phys. Rev. Lett. **50**, 1611 (1983).
[6] S. M. Anlage, H. S. Howard, J. Snortland, S. Tahara, B. Langley, C. B. Eom, and M. R. Beasley, Appl. Phys. Lett. **54**, 2710 (1989).
[7] S. M. Anlage, B. W. Langley, G. Deutscher, J. Halbritter, and M. R. Beasley, Phys. Rev. B **44**, 9764 (1991).
[8] J. Y. Lee and T. R. Lemberger, Appl. Phys. Lett. **62**, 2419 (1993).
[9] S. D. Brorson, R. Buhleier, J. O. White, I. E. Trofimov, H.-U. Habermeier, and J. Kuhl, Phys. Rev. B **49**, 6185 (1994).
[10] S. Cho, J. Korean Phys. Soc. **31**, 337 (1997).
[11] F. S. Jelila, J.-P. Maneval, F.-R. Ladan, F. Chibane, A. Marie-de-Ficquelmont, L. Mechin, J.-C. Villegier, M. Aprili, and J. Lesueur, Phys. Rev. Lett. **81**, 1933 (1998).
[12] M. N. Kunchur, Mod. Phys. Lett. B **9**, 399 (1995).
[13] M. N. Kunchur, J. Phys. Condens. Matter **16**, R1183 (2004).
[14] T. R. Lemberger, I. Hetel, J. W. Knepper, and F. Y. Yang, Phys. Rev. B **76**, 094515 (2007).